IEEE Photonics Journal
An IEEE Photonics Society Publication

Stable Gain-Guided Soliton Propagation in a Polarized Yb-Doped Mode-Locked Fiber Laser

Volume 4, Number 3, June 2012

M. E. V. Pedersen
E. J. R. Kelleher
J. C. Travers
Z. Sun
T. Hasan
A. C. Ferrari
S. V. Popov
J. R. Taylor

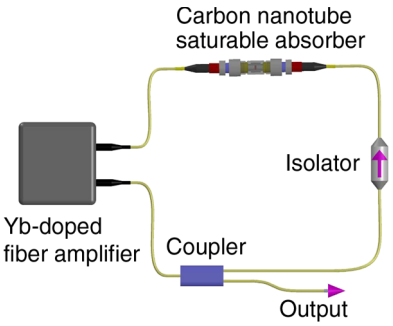

DOI: 10.1109/JPHOT.2012.2202314
1943-0655/$31.00 ©2012 IEEE

Stable Gain-Guided Soliton Propagation in a Polarized Yb-Doped Mode-Locked Fiber Laser

M. E. V. Pedersen,[1] E. J. R. Kelleher,[1] J. C. Travers,[1] Z. Sun,[2] T. Hasan,[2] A. C. Ferrari,[2] S. V. Popov,[1] and J. R. Taylor[1]

[1]Femtosecond Optics Group, Department of Physics, Imperial College, London SW7 2AZ, U.K.
[2]Department of Engineering, University of Cambridge, Cambridge CB3 0FA, U.K.

DOI: 10.1109/JPHOT.2012.2202314
1943-0655/$31.00 ©2012 IEEE

Manuscript received May 18, 2012; accepted May 25, 2012. Date of publication June 6, 2012; date of current version June 26, 2012. FOG is supported by the UK EPSRC and Royal Society. SVP is a Royal Society Industry Fellow, JRT and ACF are Royal Society Wolfson Research Merit Award holder. ACF acknowledges funding from the ERC Grant NANOPOTS and EPSRC Grant EP/GO30480/1. Corresponding author: E. J. R. Kelleher (e-mail: edmund.kelleher08@imperial.ac.uk).

Abstract: We demonstrate gain-guided dissipative soliton operation of a linearly polarized Yb-doped fiber laser, mode-locked by carbon nanotubes. In the regime of low nonlinear phase shift per cavity roundtrip, a dissipative soliton pulse can be supported by the finite gain bandwidth, without the need for strong spectral selection. The gain-guiding dynamics are confirmed by simulations.

Index Terms: Mode locking, fiber lasers, nanotubes, nanocomposites.

Stable, polarized fiber lasers with compact and simple design are in great demand for a variety of applications, such as spectroscopy, wavelength conversion, and optical communications [1], [2]. Yb-doped fibers, having broad gain bandwidth, are an attractive medium for ultrafast pulse generation. Previously, such lasers required complex dispersion-compensation setups [3], [4]. It is now routine to operate Yb fiber lasers without dispersion compensating elements, in the normally dispersive regime, to overcome the limits imposed by conservative soliton propagation [4]. A large body of work, both theoretical and experimental, has been devoted to understanding the evolution of pulse structures in such dissipative systems [4]–[8]. Instead of the usual dynamic of a balance between anomalous group velocity dispersion (GVD) and electronic Kerr nonlinearity [4], leading to the stable formation of a solitary wave [4], as in a soliton laser [4], all-normal dispersion (ANDi) systems support temporal dissipative solitons, characterized by an internal energy flow that underlies the balance of amplitude and phase modulation needed to form a soliton-pulse solution [4], [5]. Hence, the pulse shaping mechanism in ANDi lasers is strongly dependent on dissipative processes, such as linear gain (and loss) and nonlinear saturable absorption, resulting in self-amplitude modulation [4], [5].

Currently, ultrafast ANDi lasers generating chirped pulses typically need intracavity filters to mimic the action of a saturable absorber (SA), maintaining pulse formation in the steady-state [4]. Such components (e.g., free-space [4] or fiber [9] based) can give rise to extra instabilities [2] and increase the system complexity [2]. However, previous works [10]–[12] have shown that the need for a discrete filtering element can be relaxed in certain cases, leading to the formation of so-called "gain-guided" solitons. In such cases, additional filter components are not needed. In Ref. [10], the relatively narrow-bandwidth of the Erbium gain profile (around the peak at 1530 nm) provided

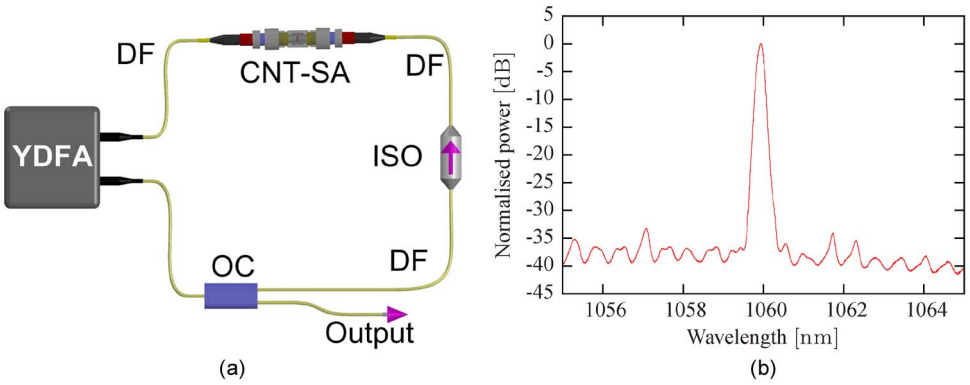

Fig. 1. Overview of our ring cavity and measured output spectrum. (a) Scheme of our ring cavity. YDFA, Yb-doped fiber amplifier; CNT-SA, nanotube-based saturable absorber; OC, output coupler; ISO, isolator; DF, dispersive fiber. (b) Output spectrum, measured with a 0.01 nm resolution.

sufficient gain dispersion to support the formation of a dissipative soliton pulse. In Ref. [11], it was reported that an artificial birefringent filter, intrinsic to the nonlinear polarization evolution (NPE) technique used as a pseudo-SA, provided sufficient spectral limitation even for a broad gain bandwidth. NPE was also used in Ref. [12], in combination with a semiconductor SA mirror (SESAM), and it was argued that the intrinsic birefringent filtering effects also contributed to pulse shaping.

NPE is widely exploited to mode-lock ANDi lasers, allowing scalability of pulse energy, without damage to passive components [13]. However, such systems can suffer instabilities due to environmental fluctuations [4], [5], [10], [14]. In addition, polarization-maintaining (PM) fibers, which can offer increased stability [15] and a polarized output, are not employable in NPE lasers [2]. Carbon nanotubes (CNTs) [16]–[24] and graphene [23]–[26] emerged as novel promising SAs, due to their low fabrication cost, subpicosecond recovery time [23], [26], [29], broad wavelength operation range [16], [25], low saturation power [16], [25], polarization insensitivity [23], [26], and mechanical and environmental robustness [24], [27], [28].

Here, we report a stable, low-noise, polarized, gain-guided, ANDi Yb-doped fiber laser, mode-locked by CNTs. We investigate the role of spectral filtering on the stabilization of valid pulse solutions, and show that gain-guided dissipative soliton pulses can be supported, with single-pass gain bandwidth up to ~55 nm. The birefringent filtering effect, intrinsic to NPE lasers [11], [12], is not present in our laser, due to the PM cavity, thus does not contribute to pulse shaping, in contrast to [11], [12]. In addition, although our gain bandwidth is larger than that reported in Ref. [10], our laser produces a stable, polarized short pulse output, without need of discrete filtering, in a simple, compact all-fiber configuration, where the gain dispersion is the dominant spectral limitation.

The schematic of our setup is shown in Fig. 1(a). The cavity consists of 0.9 m PM double-clad Yb-doped fiber pumped with a 4 W multimode diode laser at 980 nm; a broadband output coupler, with a 3 dB transmission bandwidth greater than 150 nm, which couples 30% of the light out; and a CNT-based SA (CNT-SA) [20], [23], adhered to the facet of a FC-PC with index matching gel, and butt coupled to a second fiber connector with physical contact (FC-PC) forming a transmission-style device (using a fiber connector with angled physical contact (FC-APC) eliminates cavity effects introduced by the device). The length of the cavity passive fiber is 5.35 m, including the contribution from the coupler in the ring. The operation wavelength of CNT-SAs depends on the CNT bandgap [16], [23]. To match the operation wavelength of Yb-doped fiber lasers (~1060 nm), CNTs with ~0.8 nm diameter are required [30]. Therefore, we use single-wall carbon nanotubes produced by catalytic decomposition of CO on bimetallic Co-Mo catalysts (CoMoCaT) [31]. The sample predominantly consists of (6,5), (7,5), (7,6) tubes, as determined by Raman spectroscopy [32], transmission electron microscopy (TEM) [31] and photoluminescence [33]. The tube diameter is ~0.75–0.9 nm, corresponding to a 1–1.3 eV gap [30]. The CNT-SA is then fabricated as follows [23]. 2 mg CNTs are sonicated in 20 ml deionized (DI) water for 2 hr. The dispersion is then

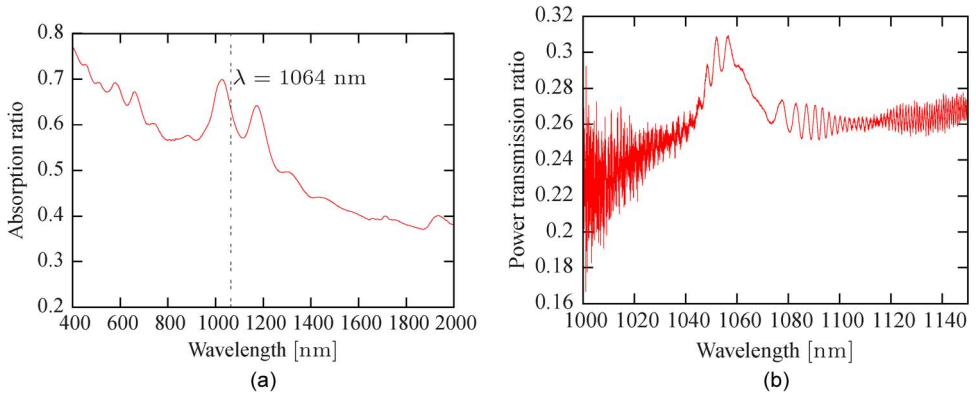

Fig. 2. CNT-SA spectral properties. (a) Absorption of CNT composite film. (b) Power transmission through the CNT-SA and the two FC-APC connectors.

centrifuged at 20 000 g using a MLA-80 fixed-angle rotor (Beckman) for 2 hr, and the top 70% decanted to obtain an aggregation-free CNT dispersion. This is then mixed with a polyvinyl alcohol (PVA) solution in DI water with a homogenizer and drop cast in a Petri dish. Slow evaporation in a desiccator yields a 50 μm CNT-polymer composite. Its absorption spectrum is plotted in Fig. 2(a). This shows a peak $\sim$1028 nm, close to the desired operation wavelength, in correspondence to the first transition of (6,5) and (7,5) CNTs with 0.76 and 0.83 nm diameters [30]. Another band $\sim$1170 nm is seen, due to 0.89 nm (7,6) CNTs [30].

We record our data when the laser is mode-locked and in a stable single pulse mode of operation. Our laser can maintain the same stable state over several-hours without readjustment of the cavity pump power. The output power is -1.4 dBm. If the pump power is increased even further the pulse operation becomes unstable, and for even higher pump power the laser begins to multipulse. Fig. 1(b) plots the output spectrum for stable single pulse operation. Without a discrete spectral filter, and within a specific power range above threshold, the laser operates with more than one line oscillating. However, in single pulse operation the laser works at 1060 nm, with a 3 dB bandwidth of 0.15 nm. The low level oscillations present in the spectrum are due to a Fabry–Pérot (FP) effect at the interface between the CNT-SA and the fiber. However, because of the low finesse ($<$ 4% at each interface, due to Fresnel reflections) this has very weak filtering effects. The power transmission of our CNT-SA is measured using a low-power broadband amplified spontaneous emission (ASE) source over the spectral range 1000 to 1140 nm, and the response curve is plotted in Fig. 2(b). Small ($\sim$2%) periodic modulations due to the resonant cavity formed in the CNT-SA are seen.

The accumulated nonlinear phase shift (Φ_{NL}) per cavity pass, which is proportional to the field peak power inside the cavity, is important to the mode of laser operation, and the resulting pulse spectral and temporal profiles. Refs. [5], [6], [14], and [34] classified the properties of pulse solutions in such lasers for a range of Φ_{NL}. Here, we operate in a low intracavity peak power regime, consequently a small self-phase modulation broadens the spectrum, but the accumulated nonlinear phase shift is small $(\Phi_{NL} \ll \pi)$. Our spectral shape is consistent with the classifications outlined in Ref. [5] for lasers of this type, with normal dispersion maps.

Fig. 3(a) plots the output pulse autocorrelation. It can be well fit with a sech^2 lineshape, with a full-width at half-maximum (FWHM) temporal duration of 13.9 ps. The time-bandwidth product is 1.11, which shows that the pulses are chirped, as typical for mode-locked fiber lasers with normal dispersion maps [4], [27].

Fig. 4 is a measurement of the relative intensity noise (RIN). The cavity repetition rate is 33.033 MHz, which corresponds to the round-trip time. Slower modulations of the pulse train amplitude are not observed. The RIN is -177 dBc/Hz, with a peak to pedestal extinction ratio of 57 dB. From $\Delta E = \sqrt{\Delta P \Delta f / \Delta f_{Res}}$ [35], where ΔE the relative pulse-to-pulse energy fluctuation (defined as output pulse energy change divided by the average output energy), ΔP is the signal-to-noise

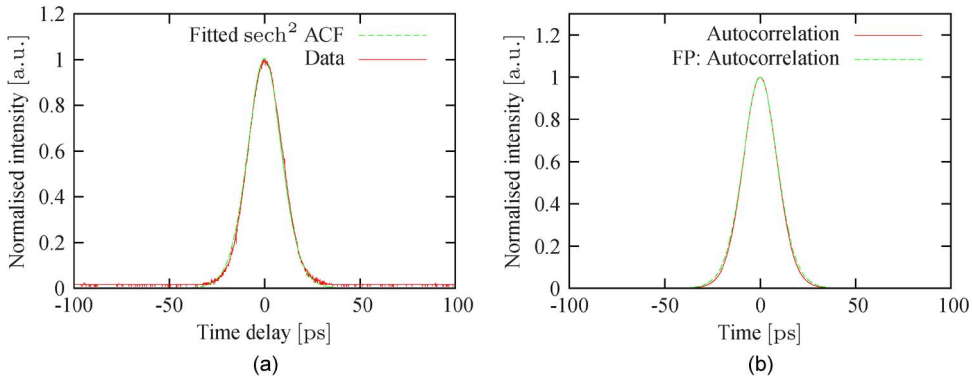

Fig. 3. Measured and simulated autocorrelations. (a) Autocorrelation. The FWHM is 21.4 ps. ACF: autocorrelation function. (b) Autocorrelation of the simulated output pulse in the time domain. FP is the simulation with the Fabry–Pérot element included. The FWHM is 21.2 ps with the FP, and 20.9 ps without.

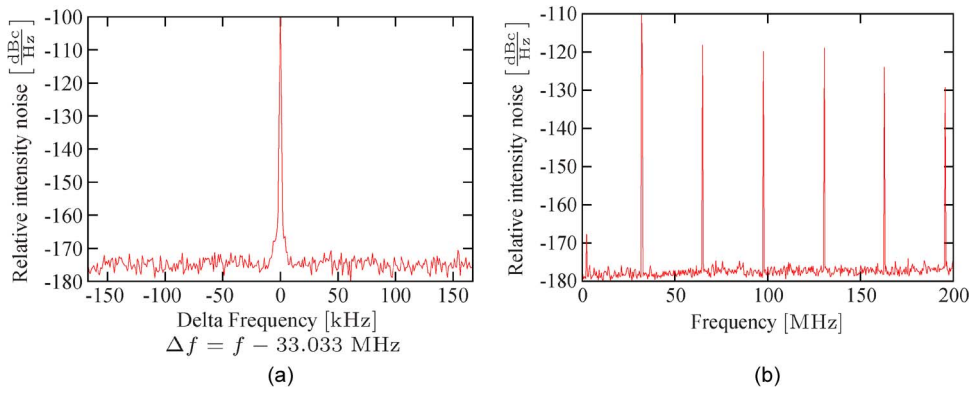

Fig. 4. Radio frequency spectrum measurement. (a) Spectrum at fundamental harmonic. (b) Spectrum with 200 MHz span.

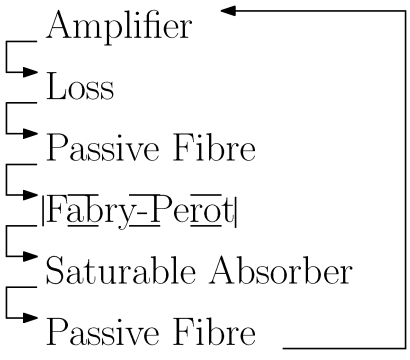

Fig. 5. Scheme of our simulation approach. The simulation without Fabry-Perot effect (marked with dashed line) is also carried out.

ratio of the peak spectrum, Δf (Hz), Δf_{Res} (Hz) are the spectral width and resolution, the calculated ΔE from the fundamental harmonic is 3.6×10^{-3}, highlighting the stability of our pulses.

To investigate the dynamics of the cavity in further detail and to probe the influence of the intracavity filtering effects, we perform numerical simulations of the laser system, with and without the FP effect from the CNT-SA interface, as outlined in Fig. 5. We solve the nonlinear Schrödinger

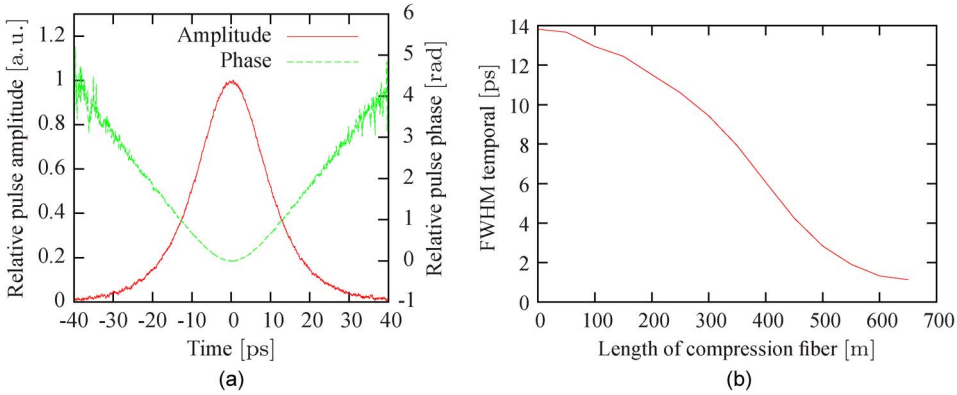

Fig. 6. Temporal output pulse and numerical compression. (a) Temporal amplitude and phase for the simulated output pulse with FP. (b) Numerical compression of the output pulse for a fiber with dispersion $\beta_2 = -0.018$ ps^2/m and nonlinear coefficient 0.003 1/Wm. The estimated chirp is $\sim$11.7 ps^2.

equation for the different cavity components and use the output from one component as input to the other. The simulation is started from noise. A stable pulse is obtained after some thousand iterations. The Raman effect [2] is disregarded due to our small pulse bandwidth. We consider a pulse centered at 1060 nm with a time window of 200 ps divided into 2^{12} points and a doped fiber with length 0.9 m, dispersion $\beta_2 = 0.018$ ps^2/m, gain bandwidth of 56.8 nm, small signal gain of 20 dB. We assume a saturation energy of 90 pJ with FP, and 60 pJ without FP, as well as a nonlinear coefficient of 0.003 1/Wm. A 7 dB loss element represents contributions from the output coupler and the additional losses in the cavity. The two passive fiber components are identical, with a length 2.675 m, a dispersion $\beta_2 = 0.018$ ps^2/m, and a nonlinear coefficient 0.003 1/Wm. We model the CNT-SA with a modulation depth of 0.10, a saturation power 4.2 W for the FP case, and 2.3 W without FP, a linear loss of 0.5, based on measurements of similar CNT-SAs [17]. When included, the FP has a reflectivity of 4% and a wavelength spacing of 1.2 nm between peaks.

It is possible to numerically obtain mode-locking in a single pulse regime without a bandpass filter, both with and without FP. Fig. 3(b) plots the temporal autocorrelation of the pulse extracted at the coupler position. The temporal duration and shape match those of our physical system very well, showing that dissipative soliton pulses can be supported by a cavity where a broad gain bandwidth (such as Yb) is the dominant spectral profile. The average output power in the simulated cavity is -2.90 dBm for the FP case, and -2.94 dBm without. Fig. 6(a) plots the pulse amplitude and phase for the FP case to show the temporal chirp associated with our ANDi ring cavity. In Fig. 6(b) the output pulse is numerically compressed. This further confirms the mode-locking operation of our laser. The estimated chirp is $\sim$11.7 ps^2.

Fig. 7(a) is the pulse extracted at the coupler position in the frequency domain. With FP the spectral bandwidth is 0.19 nm, and the background spectral oscillations observed experimentally [Fig. 1(b)] are reproduced. Without FP, the bandwidth increases to 0.60 nm and the oscillations disappear. To identify the FP role on the cavity dynamics, Fig. 7(b) plots the FWHMs in both temporal and spectral domains for a pulse over one cavity evolution in the steady-state mode-locking regime. The FP has only a small effect on the overall temporal dynamics. Although the simulations with FP are more accurate, as they are closer to the physical system, the comparison with experiments indicates that the FP effect is just to narrow the spectrum and introduce background oscillations, rather than significantly influence the mode-locked operation dynamics. Fig. 7(c) reports the evolution of pulse formation without FP, with a stable pulse forming after 2000 round trips. To confirm the gain-guiding effect of the gain fiber, we perform a simulation with constant gain spectrum, i.e., without the spectral filtering of the gain fiber, Fig. 7(d). As expected, this gives no stable pulse.

In conclusion, we demonstrated stable, dissipative soliton, gain-guided operation in a polarized Yb-doped fiber laser, mode-locked using nanotubes. It is possible to support a stable pulse by

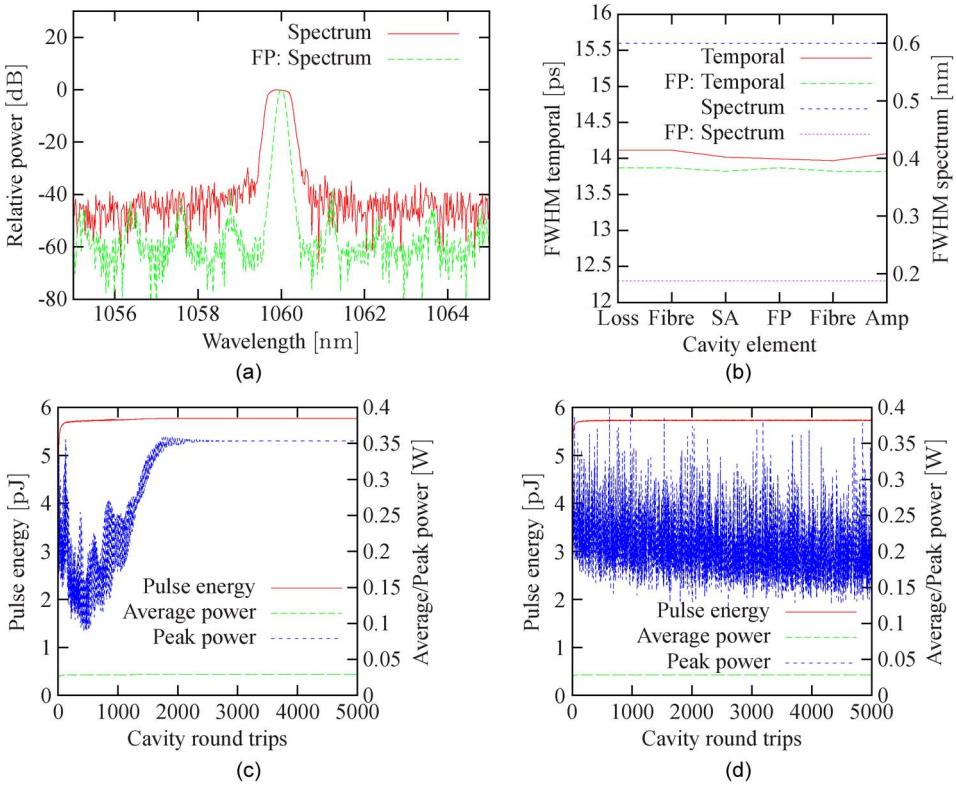

Fig. 7. Simulation results. (a) Simulated output pulse in the frequency domain. FP is the simulation with the Fabry–Pérot element. The 3 dB bandwidth is 0.19 nm with FP and 0.60 nm without. (b) FWHM in the temporal and spectral domain through the cavity element, when the pulse has mode-locked. FP is the simulation with the Fabry–Pérot element. (c) Simulated pulse average and peak power as a function of round trip, for a parabolic gain spectrum with 55 nm bandwidth. (d) Simulated pulse average and peak power as a function of round trip with constant gain spectrum.

operating in the positive dispersion regime, without soliton-shaping or a bandpass filter for stabilization. The dominating spectral selection effect comes from the gain medium, indicating that we have gain-guided mode-locked laser operation. We have also shown that transmission-style SA devices of finite thickness form a FP resonator that has a small, but noticeable effect on the laser output by narrowing the spectrum. However, this natural filter does not influence the initial pulse formation dynamics, and simulations confirm that a stable pulse can arise with or without this element.

References

[1] M. E. Fermann, A. Galvanauskas, and G. Sucha, *Ultrafast Lasers Technology and Applications*. New York: Marcel Dekker, 2003.
[2] G. P. Agrawal, *Applications of Nonlinear Fiber Optics*. London, U.K.: Academic, 2001.
[3] F. O. Ilday, J. R. Buckley, W. G. Clark, and F. W. Wise, "Self-similar evolution of parabolic pulses in a laser," *Phys. Rev. Lett.*, vol. 92, no. 21, pp. 213902-1–213902-4, May 2004.
[4] F. W. Wise, A. Chong, and W. H. Renninger, "High-energy femtosecond fiber lasers based on pulse propagation at normal dispersion," *Laser Photon. Rev.*, vol. 2, no. 1/2, pp. 58–73, Apr. 2008.
[5] A. Chong, W. H. Renninger, and F. W. Wise, "Properties of normal-dispersion femtosecond fiber lasers," *J. Opt. Soc. Amer. B*, vol. 25, no. 2, pp. 140–148, Feb. 2008.
[6] A. Chong, J. Buckley, W. Renninger, and F. Wise, "All-normal-dispersion femtosecond fiber laser," *Opt. Exp.*, vol. 14, no. 21, pp. 10 095–10 100, Oct. 2006.
[7] M. Baumgartl, F. Jansen, F. Stutzki, C. Jauregui, B. Ortac, J. Limpert, and A. Tünnermann, "High average and peak power femtosecond large-pitch photonic-crystal-fiber laser," *Opt. Lett.*, vol. 36, no. 2, pp. 244–246, Jan. 2011.
[8] B. Ortac, M. Plötner, J. Limpert, and A. Tünnermann, "Pulse dynamics in a passively mode-locked chirped-pulse fiber laser," *Appl. Phys. B*, vol. 99, no. 1/2, pp. 79–82, Apr. 2010.

[9] K. Kieu and F. W. Wise, "All-fiber normal-dispersion femtosecond laser," *Opt. Exp.*, vol. 16, no. 15, pp. 11 453–11 458, Jul. 2008.
[10] L. M. Zhao, D. Y. Tang, H. Zhang, T. H. Cheng, H. Y. Tam, and C. Lu, "Dynamics of gain-guided solitons in an all-normal-dispersion fiber laser," *Opt. Lett.*, vol. 32, no. 13, pp. 1806–1808, Jul. 2007.
[11] L. Zhao, D. Tang, X. Wu, and H. Zhang, "Dissipative soliton generation in Yb-fiber laser with an invisible intracavity bandpass filter," *Opt. Lett.*, vol. 35, no. 16, pp. 2756–2758, Aug. 2010.
[12] M. Baumgartl, B. Ortaç, C. Lecaplain, A. Hideur, J. Limpert, and A. Tünnermann, "Sub-80 fs dissipative soliton large-mode-area fiber laser," *Opt. Lett.*, vol. 35, no. 13, pp. 2311–2313, Jul. 2010.
[13] S. Lefrancois, K. Kieu, Y. Deng, J. D. Kafka, and F. W. Wise, "Scaling of dissipative soliton fiber lasers to megawatt peak powers by use of large-area photonic crystal fiber," *Opt. Lett.*, vol. 35, no. 10, pp. 1569–1571, May 2010.
[14] W. H. Renninger, A. Chong, and F. W. Wise, "Dissipative solitons in normal-dispersion fiber lasers," *Phys. Rev. A*, vol. 77, no. 2, pp. 023814-1–023814-4, Feb. 2008.
[15] X. Liu, J. Laegsgaard, and D. Turchinovich, "Highly-stable monolithic femtosecond Yb-fiber laser system based on photonic crystal fibers"," *Opt. Exp.*, vol. 18, no. 15, pp. 15 475–15 483, Jul. 2010.
[16] F. Wang, A. G. Rozhin, V. Scardaci, Z. Sun, F. Hennrich, I. H. White, W. I. Milne, and A. C. Ferrari, "Wideband-tuneable, nanotube mode-locked, fibre laser," *Nat. Nanotechnol.*, vol. 3, no. 12, pp. 738–742, Dec. 2008.
[17] J. C. Travers, J. Morgenweg, E. D. Obraztsova, A. I. Chernov, E. J. R. Kelleher, and S. V. Popov, "Using the e_{22} transition of carbon nanotubes for fiber laser mode-locking," *Laser Phys. Lett.*, vol. 8, no. 2, pp. 144–149, Feb. 2011.
[18] Z. Sun, T. Hasan, F. Wang, A. G. Rozhin, I. H. White, and A. C. Ferrari, "Ultrafast stretched-pulse fiber laser mode-locked by carbon nanotubes," *Nano Res.*, vol. 3, no. 6, pp. 404–411, 2010.
[19] E. J. R. Kelleher, J. C. Travers, Z. Sun, A. G. Rozhin, A. C. Ferrari, S. V. Popov, and J. R. Taylor, "Nanosecond-pulse fiber lasers mode-locked with nanotubes," *Appl. Phys. Lett.*, vol. 95, no. 11, pp. 111108-1–111108-3, Sep. 2009.
[20] E. J. R. Kelleher, J. C. Travers, E. P. Ippen, Z. Sun, A. C. Ferrari, S. V. Popov, and J. R. Taylor, "Generation and direct measurement of giant chirp in a passively mode-locked laser," *Opt. Lett.*, vol. 34, no. 22, pp. 3526–3528, Nov. 2009.
[21] E. J. R. Kelleher, J. C. Travers, Z. Sun, A. C. Ferrari, K. M. Golant, S. V. Popov, and J. R. Taylor, "Bismuth fiber integrated laser mode-locked by carbon nanotubes," *Laser Phys. Lett.*, vol. 7, no. 11, pp. 790–794, Nov. 2010.
[22] C. E. S. Castellani, E. J. R. Kelleher, J. C. Travers, D. Popa, T. Hasan, Z. Sun, A. C. Ferrari, S. V. Popov, and J. R. Taylor, "Ultrafast Raman laser mode-locked by nanotubes," *Opt. Lett.*, vol. 36, no. 20, pp. 3996–3998, Oct. 2011.
[23] T. Hasan, Z. Sun, F. Wang, F. Bonaccorso, P. H. Tan, A. G. Rozhin, and A. C. Ferrari, "Nanotube-polymer composites for ultrafast photonics," *Adv. Mater.*, vol. 21, pp. 3874–3899, 2009.
[24] Z. Sun, T. Hasan, and A. C. Ferrari, "Ultrafast lasers mode-locked by nanotubes and graphene," *Phys. E*, vol. 44, no. 6, pp. 1082–1091, Mar. 2012, DOI: 10.1016/j.physe.2012.01.012.
[25] Z. Sun, T. Hasan, F. Torrisi, D. Popa, G. Privitera, F. Wang, F. Bonaccorso, D. M. Basko, and A. C. Ferrari, "Graphene mode-locked ultrafast laser," *ACS Nano*, vol. 4, no. 2, pp. 803–810, Feb. 2010.
[26] F. Bonaccorso, Z. Sun, T. Hasan, and A. C. Ferrari, "Graphene photonics and optoelectronics," *Nat. Photon.*, vol. 4, no. 9, pp. 611–622, Sep. 2010.
[27] Z. Sun, A. G. Rozhin, F. Wang, T. Hasan, D. Popa, W. O'Neill, and A. C. Ferrari, "A compact, high power, ultrafast laser mode-locked by carbon nanotubes," *Appl. Phys. Lett.*, vol. 95, no. 25, pp. 253102-1–253102-3, Dec. 2009.
[28] Z. Sun, D. Popa, T. Hasan, F. Torrisi, F. Wang, E. Kelleher, J. Travers, V. Nicolosi, and A. Ferrari, "A stable, wideband tunable, near transform-limited, graphene-mode-locked, ultrafast laser," *Nano Res.*, vol. 3, no. 9, pp. 653–660, 2010.
[29] D. Popa, Z. Sun, F. Torrisi, T. Hasan, F. Wang, and A. C. Ferrari, "Sub 200 fs pulse generation from a graphene mode-locked fiber laser," *Appl. Phys. Lett.*, vol. 97, no. 20, pp. 203106-1–203106-3, Nov. 2010.
[30] R. B. Weisman and S. M. Bachilo, "Dependence of optical transition energies on structure for single-walled carbon nanotubes in aqueous suspension: An empirical Kataura plot," *Nano Lett.*, vol. 3, no. 9, pp. 1235–1238, Sep. 2003.
[31] B. Kitiyanan, W. E. Alvarez, J. H. Harwell, and D. E. Resasco, "Controlled production of single-wall carbon nanotubes by catalytic decomposition of CO on bimetallic Co-Mo catalysts," *Chem. Phys. Lett.*, vol. 317, no. 3–5, pp. 497–503, Feb. 2000.
[32] A. Jorio, A. P. Santos, H. B. Ribeiro, C. Fantini, M. Souza, J. P. M. Vieira, C. A. Furtado, J. Jiang, R. Saito, L. Balzano, D. E. Resasco, and M. A. Pimenta, "Quantifying carbon-nanotube species with resonance Raman scattering," *Phys. Rev. B*, vol. 72, no. 7, pp. 075207-1–075207-5, Aug. 2005.
[33] S. M. Bachilo, L. Balzano, J. E. Herrera, F. Pompeo, D. E. Resasco, and R. B. Weisman, "Narrow (n, m)-distribution of single-walled carbon nanotubes grown using a solid supported catalyst," *J. Amer. Chem. Soc.*, vol. 125, no. 37, pp. 11 186–11 187, Sep. 2003.
[34] B. G. Bale, J. N. Kutz, A. Chong, W. H. Renninger, and F. W. Wise, "Spectral filtering for high-energy mode-locking in normal dispersion fiber lasers," *J. Opt. Soc. Amer. B*, vol. 25, no. 10, pp. 1763–1770, Oct. 2008.
[35] D. Linde, "Characterization of the noise in continuously operating mode-locked lasers," *Appl. Phys. B, Lasers Opt.*, vol. 39, no. 4, pp. 201–217, Apr. 1986.